Support Structure Design of the Nb_3Sn Quadrupole for the High Luminosity LHC

M. Juchno, G. Ambrosio, M. Anerella, D. Cheng, H. Felice, P. Ferracin, J. C. Perez, H. Prin, J. Schmalzle

***Abstract*—New low-β quadrupole magnets are being developed within the scope of the High Luminosity LHC (HL-LHC) project in collaboration with the US LARP program. The aim of the HL-LHC project is to study and implement machine upgrades necessary for increasing the luminosity of the LHC. The new quadrupoles, which are based on the Nb_3Sn superconducting technology, will be installed in the LHC Interaction Regions and will have to generate a gradient of 140 T/m in a coil aperture of 150 mm. In this paper, we describe the design of the short model magnet support structure and discuss results of the detailed 3D numerical analysis performed in preparation for the first short model test.**

***Index Terms*— bladders, High Luminosity LHC, Interaction Regions, keys, low-β quadrupoles, Nb3Sn magnets, short model, support structure.**

I. Introduction

The High-Luminosity LHC (HL-LHC) project aims at upgrading some of the components of the accelerator in order to increase the luminosity of the LHC. Among the deliverables of the project are the new low-β quadrupole magnets that will be installed in two of the LHC Interaction Regions (IRs) [1]. The design of new IR quadrupole magnet, which is referred as MQXF, is based on the Nb_3Sn superconducting technology, with a coil of 150 mm of aperture generating a gradient of 140 T/m. It is being developed and built by the collaboration between CERN and the US LHC Accelerator Research Program (LARP) based on the previous LARP quadrupole design, HQ [2], which has an aperture of 120 mm. These designs utilize the bladder-and-key technology [3] that provides preload in two steps. The first preload step is performed at room temperature and involves stretching the aluminum cylinder with water pressurized bladders in order to insert interference keys. The second preload step is provided by the shrinkage of the aluminum cylinder during the cool-down.

This paper focuses on the mechanical design of the short model of the MQXF quadrupole. Its structure will be 1.55 m long (magnetic length of 1.1 m) and it will be equipped with all accelerator features required for handling, assembly and alignment. The experience gained from the development and tests of the short model will directly feedback into the development of the full length prototypes which will be built by CERN (magnetic length of 6.8 m) and LARP (magnetic length of 4 m).

Manuscript received January 1, 20.

The HiLumi LHC Design Study is included in the High Luminosity LHC project and is partly funded by the European Commission within the Framework Programme 7 Capacities Specific Programme, Grant Agreement 284404 and by DOE via the US-LARP program.

M. Juchno (e-mail: mariusz.juchno@cern.ch), P. Ferracin, J. C. Perez, H. Prin and E. Todesco are with CERN, 1211 Geneva, Switzerland.

G. Ambrosio is with FNAL, Batavia, IL 60510 USA.

D. Cheng and H. Felice are with LBNL, Berkeley, CA 94720 USA.

M. Anerella and J. Schmalzle are with Brookhaven National Laboratory (BNL), Upton, NY 11973 USA.

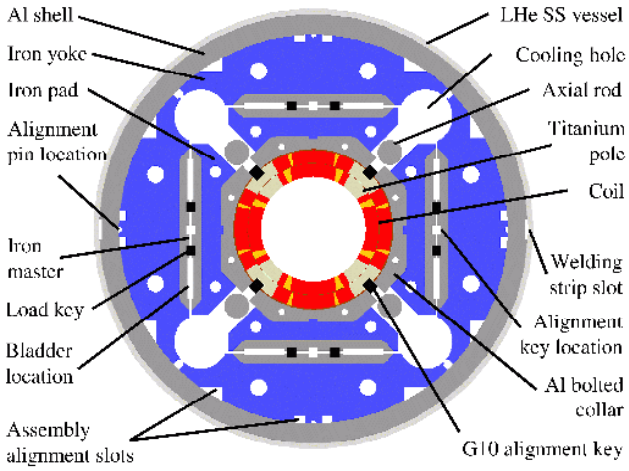

Fig. 1. MQXF magnet cross-section.

II. Update of Parameters and Cross-section

The cross-section of the MQXF magnet is designed based on the scaled up geometry of the HQ magnet with addition of features such as cooling holes, assembly and alignment slots. With respect to the initial design, which is described in details in [4], the cross-section underwent minor modifications regarding mostly the manufacturing of the structure parts, its assembly and alignment. The most relevant modification was addition of assembly cut-outs in the aluminum cylinder and

TABLE I
Coil and Magnet Parameters

Parameter	Unit	
Structure length (without axial support)	m	1.55
Magnet outer diameter	mm	630
Clear aperture diameter	mm	150
No. turns in layer 1/2 (octant)		22/28
Nominal gradient G_{nom}	T/m	140
Nominal current I_{nom}	kA	17.46
Nominal conductor peak field B_{nom}	T	12.1
Load-line margin	%	20
Stored energy density in straight sect. at I_{nom}	MJ/m	1.32
Differential inductance at I_{nom}	mH/m	8.2
F_x / F_y (per octant) at I_{nom}	MN/m	2.74 / -3.83
F_z (whole magnet) at I_{nom}	MN	1.3

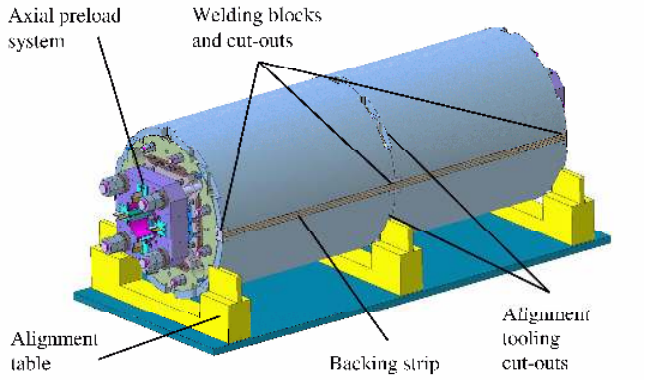

Fig. 2. Short model of the MQXF magnet.

full length slots along its horizontal mid-plane for the insertion of the welding backing-strip. This stainless steel bar will provide a link between the outer liquid helium vessel and the magnet yoke through the welding blocks bolted to the yoke at the extremity of each aluminum cylinder segment. The strip will also provide a protection of the pressure vessel weld from the aluminum contamination. The additional slot required re-optimization of the aluminum shell thickness and the interference key in order to maintain the same preload level. Fig. 1 and Fig. 2 show the final design of the MQXF short model cross-section and the 3D view of the structure while the main parameters of the magnet are listed in Table I.

III. Numerical Analysis of the Short Model

The initial analysis of the MQXF structure and optimization of its cross-section was performed with the 2D numerical analysis [4]. The 3D model of the structure was built based on the developed 2D model. Fig. 3 shows the geometry or the 3D model with its most important features of the magnet structure: 1) segmented aluminum shell with exterior cut-outs required for the magnet assembly and alignment; 2) segmented pad with central iron part and stainless steel ends for reducing the field in the magnet heads; 3) geometry of the return end of the potted coil with stainless steel end-spacers and end-shoes [5]; 4) the axial preload system.

The most important aspect covered by the 3D numerical

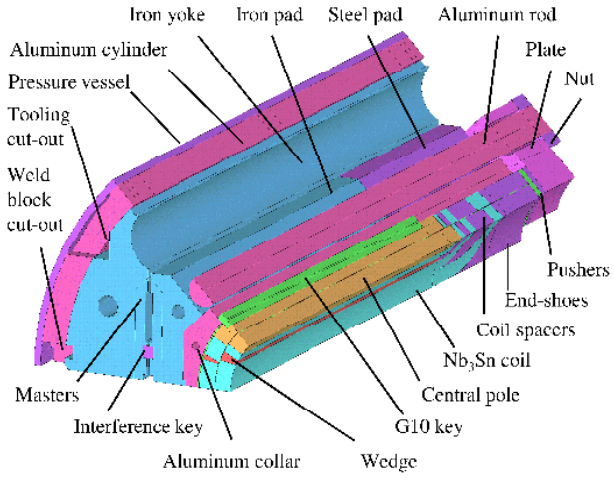

Fig. 3. Numerical 3D model of the short MQXF structure.

analysis were: the coil and the structure stress management at the preload level required to counteract the magnetic forces; dependence of the coil stress uniformity on: the axial friction between the yoke and the shell during cool-down, the size of the aluminum cylinder cut-outs, and the liquid helium vessel; design of the axial preload system and investigation of the required axial preload level.

A. Comparison of 2D and 3D Analysis Results

The optimization of the MQXF cross-section was initially performed with the 2D numerical analysis. Its goals were to manage the stress level in the coil and the structure below assumed maximum values [4] as well as to apply and distribute the coil preload to keep the coil compressed at the magnetization level at 10% above the nominal current. However, the 2D model does not take into account factors such as: 1) axial thermal contraction of the coil and the titanium pole that can lead to overestimation of the azimuthal compression of the pole-turn of the coil by the 2D model; 2) the discontinuity of the pad material and stainless steel coil spacer that introduce a local increase of the coil stress and preload; 3) variation of the coil stress and preload due to the axial thermal contraction of the shell and axial friction between the shell and the yoke.

Comparison between the 2D and the 3D analysis results is presented in Table II. The performed analysis shows that, in terms of the peak stress in the aluminum shell and the iron structure, the initial optimization remains valid when the 3D effects are taken into account. Some of these effects, such as discontinuity of the pad material, are responsible for a local increase of the peak stress in the coil in the 3D model results. Results regarding the coil preload are discussed in the next section.

B. Shell Segment Length and Coil Stress Uniformity

Past experience from magnets structures developed by the LARP program shows that due to different thermal contraction properties of the iron yoke and the aluminum cylinder, the cylinder is partially refrained from contracting in the axial direction [6]. Friction between the yoke and the aluminum shell causes high axial stress of the shell after cool-down and risk of sudden shell slippage during the coil magnetization [6]. These frictional forces influence also the uniformity of the azimuthal and axial coil stress (σ_θ and σ_z) due to additional axial strain (ε_z) as shown by the following relation

$$\sigma_{\theta,z} = \frac{E}{(1-\nu^2)}\left(\varepsilon_{\theta,z} + \nu\varepsilon_{z,\theta}\right),$$

where E and ν are, respectively, the elastic modulus and the

TABLE II
Comparison of 2D and 3D Models

Component	2D	3D
Coil $\sigma_\Theta^{RT/CD/MF}$ (MPa)	-70 / -170 / -161	-76 / -196 / -173
Shell $\sigma_\Theta^{RT/CD/MF}$ (MPa)	136 / 264 / 272	140 / 276 / 274
Iron $\sigma_{eqv}^{RT/CD/MF}$ (MPa)	144 / 266 / 274	157 / 300 / 307

Maximum stress values at different steps of magnet assembly and operation: after key insertion at room temperature (RT); after cool-down (CD); with magnetic forces (MF).

Poisson's ratio [6]. Therefore, it is necessary to study the behavior of the structure with the segmented shell [7] especially taking into account the future long model development.

Two scenarios were analyzed, where the aluminum cylinder forms a single segment of 1.55 m and when it is divided into two segments of 0.775 m. In both cases, analyzed shells did not have assembly cut-out at their extremities. The division of the shell segment allowed to decrease the axial stress from 90 to 45 MPa and to reduce the variation of the azimuthal stress from ±11 MPa to approximately ±6 MPa. Azimuthal and axial stress distributions along the shell segments are presented in Fig. 4.

In addition to abovementioned advantages, utilizing at least two shell segments for the short model design is important in terms of the coil stress analysis. Since the structure of the MQXF short model is 1.55 m long, a single shell of the same length as the structure would not allow to study the coil stress variation in similar conditions as in the long model. The entire straight section of the coil would be located in the central part of the shell segment and would not experience the full possible range of the preload variation. Therefore, the numerical analysis summarized in Fig. 5 was focused on the case with 0.775 m long aluminum shell segments.

The model was set up in the way that it allows to analyze the case corresponding to one of the central segments of the long model (longitudinal range from 0 to 0.775 m in Fig. 5) and external segment of the long model that represents the state of the short model segment (longitudinal range from 0.775 to 1.55 m in Fig. 5).

The variation of the azimuthal stress in the coil was investigated on the mid-radius of the inner coil layer, on the surface of the pole-turn. In Fig. 5, the blue line with circular markers corresponds to a case where shell segments are modelled without assembly cut-outs. Stress variation in the long model segment is only ±7 MPa because there is no longitudinal material discontinuity within that segment. In the short model segment, the stress variation is ±16 MPa due to the material discontinuity in the end of the structure and the fact that the end of the coil straight section is located in the central part of the shell segment, where the contribution of the axial frictional forces is the strongest.

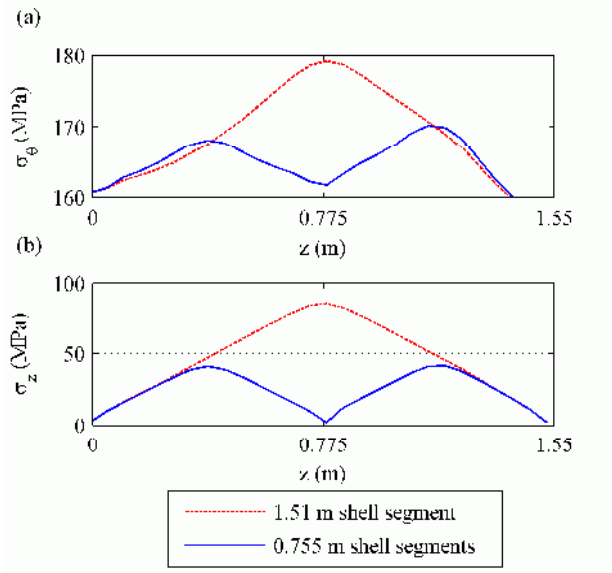

Fig. 4. Azimuthal (a) and axial (b) stress in aluminum cylinder segments after cool-down.

The coil stress calculated with the 2D numerical model was shown in Fig. 5 as magenta line with diamond markers. Two important factors contribute to the discrepancy with respect the 3D analysis results (blue line). The 2D analysis does not take into account the axial tension of the coil after cool-down due to low thermal contraction of the titanium pole. It also does not allow to model the axial compression of the coil due to the axial contraction of the aluminum shell and frictional forces.

C. Shell Cut-Outs

For reasons of the magnet assembly and alignment, it is necessary to have access to the magnet yoke during the assembly procedure. Therefore a pattern of cut-outs was introduced at each extremity of the shell segment (see Fig. 2 and Fig. 3) in order to: 1) insert a welding block that is to be bolted to the yoke and links it with the external pressure vessel; 2) align the structure against the assembly bench during welding of the pressure vessel.

As the shell cut-outs reduce the preload in the area of the shell extremities, the sensitivity of the coil stress variation to these cut-outs was analyzed. The weld block cut-out and the alignment bench cut-out of the length of 25 mm increased the coil stress variation separately by 7 MPa and 13 MPa respectively. The cut-outs length for the first short model with 0.775 m long shell segment were set to 25 mm for the weld

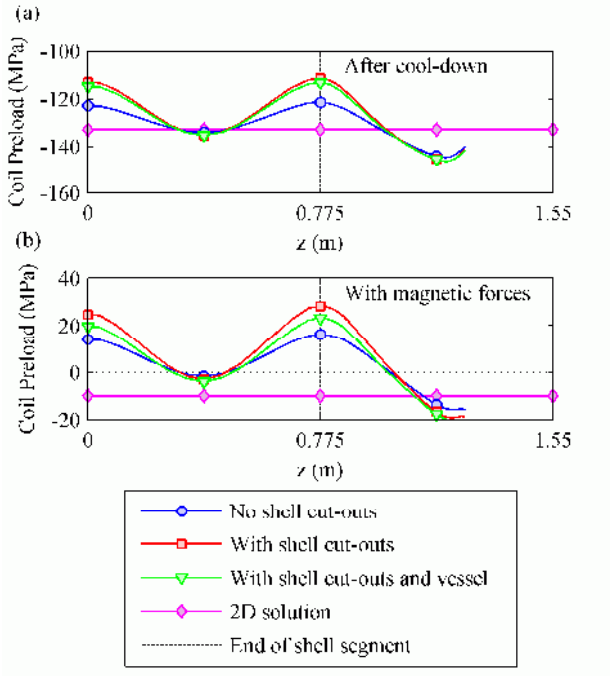

Fig. 5. Compression of the inner layer pole-turn on the mid-radius after the cool-down (a) and after powering the magnet with 90% of the short sample current I_{ss} (b). Longitudinal range from 0 to 0.755 m corresponds to one of the central segments of the long model, while the range from 0.755 to 1.51 m corresponds to the exterior segment of the long model or a segment of the short model magnet.

block cut-out and 15 mm for the alignment tooling cut-out. Estimated variation of the azimuthal coil stress (red line with square markers in Fig. 5) is ±16 MPa for the segment representative for the future long structure and ±22 MPa for the segment representative for the short structure.

D. Liquid Helium Vessel

For the installation in the machine, the MQXF will require an additional stainless steel pressure vessel for the liquid helium containment. While this vessel will not provide the preload to the structure, it has to maintain contact with the structure after the cool-down. Taking into account the difference in thermal contraction, the vessel will have to be pre-tensioned around the structure at room temperature, which can eventually affect the uniformity of the coil stress.

A vessel of 8 mm thickness and made of stainless steel 304 was modeled around the MQXF structure and pre-tensioned in room temperature to 50 MPa. The numerical analysis shows that it remains in contact with the structure after cool-down. Fig. 5a shows a positive effect of the vessel on the coil stress when magnetic forces are applied (green line with triangular markers). Compression of the coil in the area of aluminum shell extremities was improved by 5 MPa, while the effect in the central area of the shell segment was negligible. The computed coil stress variation is ±14 MPa for the segment representative for the future long structure and ±20 MPa for the segment representative for the short structure and maximum azimuthal tension in the coil is 23 MPa.

E. Axial Preload System Analysis

Structure of the MQXF provides also axial preload, which counteracts the Lorentz force of 1.3 MN (see Table I) acting on the coil ends. The axial preload system was designed so that the compressive force of the same magnitude can be applied. The preload is provided by the aluminum four axial rods of 42 mm in diameter pre-tensioned during the magnet assembly. The force is transferred through the end plates and a system of pushers, to the coil end-shoes. This results in the coil ends being compressed against the titanium pole. The nominal preload force is obtained after the cool-down due to thermal contraction of the axial rod.

Numerical analysis of the axial preload system was performed to estimate the total axial force required to compress the coil and prevent it from detaching from the pole or end-spacers. Fig. 6 shows the position of the coil blocks in the return end and the contact pressure at the extremities of the contact surfaces between the coil and the end-spacers. The total applied axial force in the presented case was 1.25 MN (0.78 MN at room temperature and 0.47 MN after cool-down). Maximum axial stress in the rods is 310 MPa.

The analysis shows that designed axial support system is capable of sufficiently preloading the coil ends and avoiding its detachment from the central pole.

IV. Conclusion

The short model of the MQXF magnet will be the first Nb_3Sn quadrupole using the shell-based structure equipped with all accelerator grade features required for the magnet alignment and installation in the LHC tunnel. With the use of the 3D numerical model, the state of the structure components and preload of the coil was studied taking into account the new magnet features.

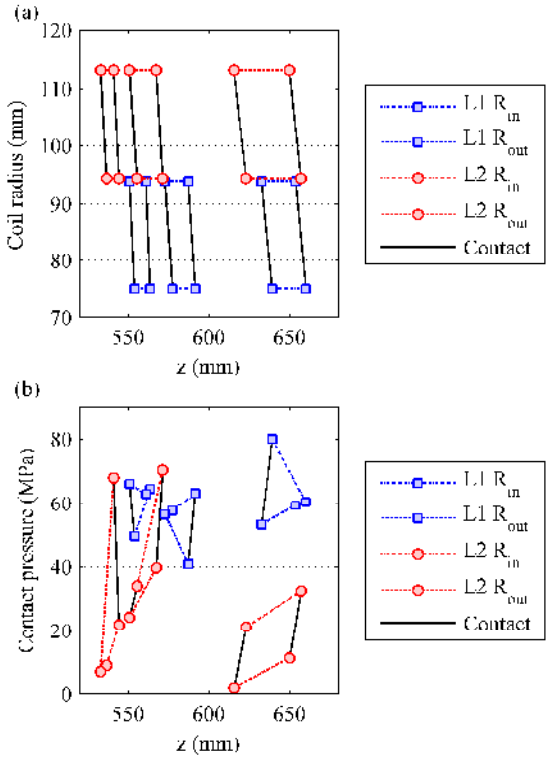

Fig. 6. Position of coil blocks in the return end with respect to the center of the coil (a). Contact pressure between the coil block and end-spacers of the return end with coil powered to 90% of the short sample current I_{ss} and the axial rod force of 1.25 MN (b).

The numerical analysis showed that, due to its length, the short MQXF model will only represent the conditions of the exterior segments of the future long magnet. These regions of the magnet are the most critical for its operation and are strongly influenced by the longitudinal discontinuity of its components, such as pads and coil spacers. The present design of the short model with the shell segment length of 0.775 m will allow to study these effects prior to the long model development.

Considering all described features in the current design of the MQXF structure, the maximum azimuthal tensions of the pole turn at 90% of the load-line is 23 MPa and the average (maximum) variation of the azimuthal stress is ±14 MPa (±20 MPa). In the axial direction, the designed axial preload system is capable of maintaining the compression of the coil ends against the pole and the coil spacers.

Acknowledgment

Authors would like to thank B. Favart and T. Sahner for providing CAD support during the magnet design.

References

[1] E. Todesco *et al.*, "A First Baseline for the Magnets in the High Luminosity LHC Insertion Regions," *IEEE Trans. Appl. Supercond.*, vol. 24, p. 4003305, June 2014.

[2] S. Caspi *et al.*, "Design of a 120 mm Bore 15 T Quadrupole for the LHC Upgrade Phase II," *IEEE Trans. Appl. Supercond.*, vol. 20, no. 3, pp. 144-147, June 2010.
[3] S. Caspi *et al.*, "*The Use of Pressurized Bladders for Stress Control of Superconducting Magnets*," *IEEE Trans. Appl. Supercond.*, vol. 11, no. 1, pp. 2272-2275, August 2002.
[4] P. Ferracin *et al.,* "Magnet design of the 150 mm aperture low-β quadrupoles for the high luminosity LHC," *IEEE Trans. Appl. Supercond.*, vol. 24, no. 3, p. 4002306, June 2014.
[5] S. Izquierdo Bermudez, *et al.,* "Coil End Optimization of the Low β quadrupole for the High Luminosity LHC," *IEEE Trans. Appl. Supercond.*, vol. 25 submitted for publication.
[6] P. Ferracin, *et al.,* "Assembly and Test of a Support Structure for 3.6 m Long Nb_3Sn Racetrack Coils," *IEEE Trans. Appl. Supercond.*, vol. 18, no. 2, pp. 167-171, June 2008.
[7] P. Ferracin, *et al.*, "Fabrication and Test of a 3.7 m Long Support Structure for the LARP Nb_3Sn Quadrupole Magnet LQS01," *IEEE Trans. Appl. Supercond.*, vol. 19, no. 3, pp. 1683-1686, June 2009.